Influence of soil-structure interaction on seismic demands of historic masonry structure of Kashan Grand Bazaar

Hossein Tahghighi (tahghighi@kashanu.ac.ir)
The University of Kashan https://orcid.org/0000-0001-6091-8815
Amir H. Lazizi
University of Kashan

Research Article

Keywords: Seismic analysis, Finite element method, Soil-structure interaction, Historical structure, Kashan Grand Bazaar.

Posted Date: May 25th, 2022

DOI: https://doi.org/10.21203/rs.3.rs-1580976/v1

Abstract

Heritable constructions are an essential portion of the history of any nation in addition to financial resources. The aim of this study is to investigate the earthquake damage and failure mechanism of a historic Bazaar located in Kashan (center of Iran), which dates to the seventeenth century. Numerical models were constructed by a macro method, considering two cases of fixed support and soil-structure interaction (SSI). To assess the structural behavior, modal, nonlinear static and dynamic time history analyses were performed using a three dimensional finite element method. The results of SSI analysis show an intense weakness of the structure against the required demand based on the design spectrum. Also, foundation flexibility has a great impact on the oscillation characteristics, displacement demand and damage distribution. By comparing the results of time history analysis to the pushover procedure, a lower shear value and higher displacement are obtained. Furthermore, the damage process is as dome collapse alongside short arc, consequently long arc collapse followed by pier wall overturning.

1. Introduction

Historical constructions illustrate a set of specific heritage, economic and social values, which can be considered as parts of integrity and continuity [1]. Nowadays, the determination of international institutions in charge of recommendations for historical monuments is to protect the integrity and significance of such buildings [2, 3]. Most heritage buildings are made of masonry that naturally has low capacity against lateral loads. In addition, seismic design concepts were usually not considered during the construction of historic structures. Thus, damage evaluation and vulnerability analysis of such structures is very crucial, especially in earthquake active areas. Because of the complications in geometry, boundary constraints, and material characteristics of historic masonry constructions, their vulnerability assessments are often carried out using numerical tools [4–8].

Page [9] developed a finite element model for masonry including material nonlinearity and failure mechanisms of the joint. Lourenço et al. [10] used contact elements to micro-model the in-plane unreinforced masonry walls. In which, the mortar joint and the masonry element are represented independently as a continuum. Because of troubles in numerical modeling and excessive computation requirements, the micro-model is appropriate for small-scale simulations [11]. Therefore, homogenization techniques are addressed, in which it is not possible to distinguish masonry units and mortar joints from each other and masonry constructions can be modeled in an integrated manner [12, 13]. The simplified macro modeling homogenized strategy is very promising in analyzing large-volume models and is applicable for the safety assessment of masonry constructions in engineering practice due to adequacy and computational efficiency.

Soil-structure interaction (SSI) is a procedure in which soil reaction influences structure movement and vice-versa [14]. Depending on the structural characteristics, the features of the subsoil, and the frequency content of input motion, ignoring the SSI effects can be beneficial or detrimental [15, 16]. In this respect, historical masonry buildings, due to limited height and stiff sections, if placed on soft soil, the SSI could have a substantial effect on dynamic features of soil-structure systems [17]. In engineering practice, two common approaches of subsoil modeling are numerical continuum methods and Winkler-based methods. Winkler's hypothesis, despite its simplicity and practicality, is basically unable to describe the actual characteristics of soil medium due to the independent assumption of overlapping soil layers, the main focus on the adjacent soil touching the foundation, and the difficult estimation of spring stiffness values [18, 19]. The numerical method, however, is the most prominent and rigorous solution to deal with complicated geometries and subsoil conditions, especially for 3D nonlinear problems [20, 21].

Housner [22] was one of the pioneers who studied the interaction of ground and buildings subjected to earthquake. Maria et al. [23] used experimental results from the Ghirlandina monitoring tower station to investigate the accuracy of simple methods for including the SSI effects. Using the Winkler method, de Silva et al. [24] studied the SSI impacts on the earthquake behavior of the monumental heritage towers. The effects of SSI on the historical masonry bridge using the continuum finite element method was assessed by Güllü and Jaf [25]. Fathi et al. [26, 27] studied the seismic behavior of the historical citadel of Tabriz and concluded that considering the SSI increases the probability of overturning, decreases the acceleration response and affects stress and deformation distributions. The influence of soil characteristics on the seismic damage of historical masonry minaret

using the continuum model and semi-infinite boundary element were investigated by Hökelekli and Al-Helwani [28]. de Silva [29] evaluated the SSI effects on the input motion measure and the required demand of masonry towers against weak to strong earthquakes using 3D finite difference method, where the foundation flexibility causes the structural demand enhancement and considerable tower tilt.

In this research, a part of the Kashan historic Bazaar with the least damage was surveyed and the geometric model was made based on the macro method [30]. Finite element code Abaqus was applied to perform 3D numerical simulations [31]. Modal, nonlinear static and time history analyses have been employed to evaluate the structural performance of the Bazaar by considering two cases of fixed support and SSI. The results of the analysis show that SSI has great influence on the vibration properties, pushover capacity, failure mechanism, base shear and displacement demands.

2. Kashan Grand Bazaar

In the ancient Persian language, the Bazaar comes in the form of “Vazar” and “Vakar”, meaning community and place for trade [32]. First, the Bazaar was formed seasonally and then weekly near large villages, and over time it changed from temporary to permanent constructions. Kashan Bazaar is one of the most famous and glorious historic Bazaars and the largest extensive monument in the center of Iran (Fig. 1). It is noteworthy that Kashan Grand Bazaar, as a national heritage with the registration number 1284 in August 1976, is on preparation into the UNESCO world heritage list. The current Bazaar was reconstructed after the severe Kashan earthquake in 1755 [35], which destroyed the old structure. The formation history of Kashan Bazaar predates to the 10th century.

As a masonry construction, Kashan Bazaar with a linear direction consists of a series of interrelated buildings and consecutive domes and arcs with a width of 3 m to 5 m as illustrated in Fig. 2. The complex structure of the Bazaar includes covered passages with abundant markets on each side; the primary path is named “Rasteh”. Domes of the main Rasteh are from arc types, which is one type of dome and arc. Dome and arc are one of the outstanding Iranian methods of arch construction [36]. Arcs which are perpendicular to the Bazaar direction are called long arcs and arcs which are in the Bazaar direction are called short arcs. Figure 3 gives the typical architectural parts of the Bazaar.

3. The Finite Element Model

The historical masonry structure under study is composed of clay bricks and lime-cement mortar. Due to the lack of a reliable experimental result, the mechanical characteristics of masonry were considered assuming a poor level of information listed in Table 1 [37]. Masonry has complex behavior and the implementation of an effective and simple model for this substance is beneath examination [38]. The specificity of every masonry unit in geometry and sort of material is one of the principal limitations in this way. Accordingly, the use of isotropic models based on damage plasticity is generally accepted for masonry [39–44]. Figure 4 shows the masonry stress-strain relationship and the damage evolution. In this model, when the masonry is unloaded at any point in the softening branch of the stress-strain curve, its unloaded response and modulus of elasticity of the material are weakened. The decrease in modulus of elasticity is indicated by two damage parameters, d_c and d_t. The amount of the damage parameters varies from zero, which represents the material without damage, to one, which represents the complete failure, and it is calculated according to the following equations:

$$\sigma_c = (1-d_c)E_0(\varepsilon_c - \varepsilon_c^{pl}) \quad (1)$$

$$\sigma_t = (1-d_t)E_0(\varepsilon_t - \varepsilon_t^{pl}) \quad (2)$$

where, σ_c = compressive stress, σ_t = tensile stress, E_0 = preliminary elasticity modulus, ε_t = tensile strain, ε_t^{pl} = plastic tensile strain, ε_c = compressive strain and ε_c^{pl} = plastic compressive strain.

Table 1: Masonry mechanical properties [37].

Compressive strength (MPa)	Tensile strength (MPa)	Poisson ratio	Elasticity modulus (MPa)	Density (kN/m^3)
2.4	0.24	0.2	1500	18

The dilation angle controls the quantity of plastic volumetric strain made in the course of plastic cutting. It is accepted that the amount of dilation angle is steady amid plastic rupture and its value for masonry is adopted equal to 10^o [39]. Eccentricity is a parameter associated with the incline of the flow potential function. In the event that zero is taken, the noted function is converted to a line; It also makes difficulties in convergence of the problem with very small amounts. σ_{b0}/σ_{c0} is biaxial to uniaxial compressive strength. A value between 1 and 1.27 is recommended for this parameter [44]. Selecting less than 1 caused a divergence, but by selecting more than 1.27 no change was found. Viscosity is a parameter that enables to preserve the solving problem after breaking and decreasing stiffness. K_c is the second stress invariant ratio and a value between 0.5 and 1 is proposed for this parameter [44]. Table 2 summarizes the parameters adopted for the damage plasticity model in the numerical simulations.

Table 2: The plastic parameters adopted for the structure model.

Eccentricity	Dilation angle (°)	σ_{b0}/σ_{c0}	K_c	Viscosity (Pa-s)
0.1	10	1.16	0.67	0.002

Table 3: Soil layer properties [45].

Layer No.	Description	Thickness (m)	Density (kN/m^3)	Cohesion (MPa)	Friction angle (°)	Moisture (%)	Void ratio (%)	Poisson ratio	Elasticity modulus (MPa)	Shear wave velocity (m/s)
1	Lean clay	3	16.5	0.07	30	13.5	19	0.33	25.8	243
2	Lean clay	3	13.6	0.10	36	17.4	29	0.34	29.1	280
3	Clayey sand	2	17.8	0.07	37	12.9	8	0.33	32.9	261
4	Lean clay	10	19.9	0.28	37	11.6	-	0.34	37.2	262
5	Lean clay	2	18.4	0.05	30	16.9	-	0.33	42.0	291

Table 3 lists the mechanical properties of the subsoil layers [45]. The Mohr–Coulomb model is taken into consideration as elasto-plastic behavior for soil [46]. This model is widely used in geotechnical studies and its accuracy for sandy soils (Bazaar site soil) has been confirmed in comparison with laboratory results [47–50]. Within this material model, fracture is managed with the maximum shear stress that depends on the normal stress (Fig. 5). The equation of the Mohr–Coulomb criterion is expressed by:

$$\tau = c + \sigma \tan(\varphi) \qquad (3)$$

where τ = shear stress, c = cohesion, σ = normal compressive stress, and φ = angle of friction of the soil material.

Geometry plays a key role in numerical modeling. In order to be more precise, two survey methods have been used in this study. First, images are taken from different distances of the selected arcs, then the images are analyzed utilizing the ImageJ computer program [51] and the size of various segments is gotten. To make certain the results are accurate, the estimates of various segments were then collected using point transfer and triangulation methods [52]. It is noted that the collected values in both methods had a good overlap with each other. From geotechnical investigations, the subsoil is taken into consideration as 5 layers and bedrock at a profundity of 20 m (Table 3). Based on previous studies [53], the length and width of the soil profile have been taken 81.5 m and 56 m, respectively. Also, 10 m was considered for both the length and width of infinite boundary elements of CIN3D8 [31]. Infinite elements were used to model the semi-infinite environment of the subsoil.

As shown in Fig. 6, the three dimensional finite element models were constructed under two different cases of SSI and fixed support. The soil-foundation interaction was described with the aid of contact elements utilizing normal and tangential behavior. The friction coefficient was set to 0.577 [45]. The stress continuation and transformation compatibility on the boundary among soil layers was taken using 1161 Tie elements [31]. 2415 and 28259 four-node tetrahedral element (C3D4) has been employed to mesh the foundation and structure above. Subsoil meshing was performed using 9364 eight-node brick elements (C3D8) as well. The finite and infinite elements used in this study are shown in Fig. 7. For the sake of implementing proper boundary conditions, the movement of the foot of the piers was closed in translation directions for the fixed support model. For the SSI case, the horizontal sides of the subsoil have been blocked perpendicular to the plane for pushover analysis. The freedom degrees of the bedrock were blocked in all three translational directions for both models, with and without SSI.

4. Validation Experiment

The primary level in finite element method is to guarantee that the numerical model works correctly. For validating the numerical method, the finite element results are compared with laboratory tests on masonry walls by Karimi et al. [43]. The masonry wall includes solid brick and mortar via one over one volumetric ratio. The damage plasticity theory was employed for nonlinear modeling of masonry. Configuration, boundary constraints, substance characteristics and applied forces have been considered in line with the experiment. Table 4 gives the characteristics of the masonry wall. Figure 8 depicts the masonry wall numerical model. A ten-node brick element (C3D10) was used for wall meshing and a four-node 3D rigid element (R3D4) was used for meshing U-shaped steel profiles. Figure 9 compares the numerical and laboratory hysteresis curves. Furthermore, Fig. 10 compares the envelope of numerical and laboratory analyses with the capacity curve from the pushover procedure. It is observed that the simulation results agree well with the laboratory measurements.

Table 4
Masonry wall characteristics for the numerical validation [43].

Length (mm)	Height (mm)	Thickness (mm)	Brick size (mm)	Elasticity modulus (MPa)	Poisson ratio
1500	1720	195	195×195×45	7500	0.15

Table 5
Selected ground motions [60].

No.	Earthquake	Year	Station	M_w	V_{s30} (m/s)	R_{jb} (km)	Horizontal components	*PGA* (g)
1	Duzce	1999	Lamont	7.1	782	25.8	1060-N	0.025
							1060-E	0.053
2	Manjil	1990	Abbar	7.4	724	12.6	ABBAR-L	0.514
							ABBAR-T	0.497
3	Tottori	2000	SMNH10	6.6	967	15.6	SMNH10NS	0.152
							SMNH10EW	0.226

5. Analyses Performed

Eigenvalue frequency analysis is a suitable method for controlling accuracy and obtaining the vibrating characteristics of the model. For an initial assessment of the structure, modal analysis was performed on two models, fixed support and SSI cases. Natural frequencies and mode shapes are calculated in accordance with equation (4).

$$\left(-\omega^2[M]+[K]\right)\{\phi\} = \{0\} \qquad (4)$$

where [*K*] = stiffness matrix, [*M*] = mass matrix, ω = eigenvalue (vibration frequency), and {ϕ}= eigenvector (mode shape). Because of the excessive functionality of the Lanczos procedure in complex problems [31], this technique is utilized for eigenproblem solutions.

Pushover is a suitable and compatible procedure for the analysis of masonry structures. The analysis result is the capacity curve wherein the upright axis describes the base shear in terms of top lateral displacement on the horizontal axis. Control points have been taken based on Figure 11, similar to Refs. [54, 55]. To perform this analysis, first the gravitational forces were taken into consideration and then the horizontal forces were applied independently on the horizontal X and Y axes of the structure. According to NTC regulations, the lateral load distribution is described using two configurations of G1 (linear distribution of acceleration at height) and G2 (steady distribution of acceleration at height). G2 and G1 configurations are usually critical in short and tall structures, respectively [55-57]. Thus, for the Bazaar model, horizontal load distribution was assumed based on the G2 configuration. The capacity curve stops on the correspondent movement of the bottom shear, identical to the peak value of 85%. The implicit integration solver has been used to conquer the numerical convergence complexities.

The vulnerability of the Bazaar structure is investigated by method N2 [58]. In this method, respectively, the multiple-degree-of-freedom system is transformed into an equivalent system with one-degree-of-freedom, the capacity curves are converted to bilinear load-displacement diagrams, and the elastic demand spectra are transformed into the inelastic demand spectra. Eventually, the inelastic demand spectra and the capacity curves are united in Acceleration Displacement Response

Spectra (ADRS). The required elastic demand spectra are extracted according to Standard 2800 [59] for two earthquake hazard levels; i.e., Design Basis Earthquake (DBE) and Maximum Credible Earthquake (MCE) with return periods of 475 and 2475 years, respectively.

Following the previously described analysis procedures, nonlinear dynamic time history analyses were carried out. Due to the lack of strong earthquake records in Kashan, three consistent record sets were carefully selected using the PEER-NGA database [60] representing possible seismic scenarios on the bedrock. These records were chosen by considering the features of historical earthquakes in the studied region, such as fault rupture mechanism, magnitude, and distance [61]. The details of selected records are given in Table 5. The vertical component of records was neglected. Earthquake records have been scaled to the reference peak ground acceleration (*PGA*) of 0.27g for the Bazaar site from seismic hazard assessment. Figure 12 presents the seismic hazard map of Kashan in terms of *PGA* on the seismic bedrock. It must be noted that earthquake waves are affected by local site conditions as they pass through the soil layers from the bedrock toward the free-field surface. Hence, in order to perform time history analysis for the fixed support model, site response analysis was performed using the scaled bedrock records and the soil layer properties in Table 3 [62]. Figure 13 shows the response spectra for 5% damping of the longitudinal (Z-direction) and transverse (X-direction) components of the scaled acceleration records on the free-field and the bedrock levels. Two orthogonal components of horizontal ground motions were applied to the model once, one on the X-axis and the other on the Z-axis, and once again vice versa. The results due to the critical case are then considered from each record set.

6. Results And Discussion

Table 6 gives the oscillation period of the structure for the ten primary modes in both SSI and fixed support cases. Regarding Table 6, the mass participation factors differ in the same modes with the effects of SSI. To verify the results, the relation of the fundamental period according to the NTC regulation, which is described as $T_1 = 0.0187h$, has been used. By placing the height of the structure, h, which is equal to 5.12 m, in the mentioned equation; 0.096 sec is obtained, which is very close to the fixed support first period from numerical analysis, which is 0.093 sec. In order to perform a preliminary study on the effect of finite element mesh size on response accuracy, frequency analysis was carried out on a large number of fixed support models with different element sizes. Figure 14 illustrates a sensitivity analysis concerning the first three vibration periods and the element number. The investigation shows that convergence is achieved once the number of finite elements is increased.

Table 6
Characteristics of the first ten vibration modes.

Mode	Base condition	Period (s)	Participation factors				
			X-Trans	Z-Trans	X-Rot	Y-Rot	Z-Rot
1	Fixed support	0.093	0.00	1.59	3.79	0.00	0.00
	SSI	0.216	0.00	1.64	15.50	0.00	0.00
2	Fixed support	0.063	0.00	0.00	0.01	0.02	0.01
	SSI	0.201	0.00	0.00	0.00	47.59	0.00
3	Fixed support	0.059	0.23	0.00	0.00	7.61	0.72
	SSI	0.176	1.56	0.00	0.00	0.00	10.52
4	Fixed support	0.058	1.06	0.00	0.01	1.46	3.38
	SSI	0.162	0.92	0.00	0.00	0.00	1.23
5	Fixed support	0.054	1.63	0.00	0.00	0.02	4.05
	SSI	0.158	0.00	0.00	0.00	0.00	0.00
6	Fixed support	0.047	0.00	0.00	0.02	1.49	0.00
	SSI	0.157	0.00	0.00	0.00	13.65	0.00
7	Fixed support	0.045	0.00	0.12	0.67	0.02	0.01
	SSI	0.152	0.00	0.04	0.87	0.00	0.00
8	Fixed support	0.041	0.00	0.00	0.06	0.36	0.04
	SSI	0.150	0.07	0.00	0.00	0.00	1.07
9	Fixed support	0.039	0.00	0.00	0.01	1.47	0.03
	SSI	0.149	0.00	0.22	11.93	0.00	0.00
10	Fixed support	0.039	0.02	0.00	0.96	0.23	0.10
	SSI	0.146	0.00	0.06	39.51	0.00	0.00

Figure 15 shows the first five shape modes for the given finite element models. It can be seen that the important modes in terms of displacement and rotation considering the SSI are different with the fixed support case. Thus, it can be concluded that the SSI affects the shape of the modes, so that by comparing the first 60 modes of both models, only two common modes were found. Table 7 shows a comparison between common modes. Accordingly, the vibration period of the modes related to the model considering SSI is much longer than the fixed support model. Period ratio is usually provided by seismic codes to evaluate the response of soil-structure systems. According to Table 7, the period ratio ranges from 2.32 to 3.26 for the first two common modes. On the other hand, the ASCE 7 standard [63] provides the period ratio as follows:

$$\frac{\tilde{T}}{T} = \sqrt{1 + \frac{K^{*}_{\text{fixed}}}{k_x} + \frac{K^{*}_{\text{fixed}} h^2}{k_\theta}} \qquad (5)$$

where $\tilde{T}$= period of the SSI model, T = fixed support period, K^{*}_{fixed}= stiffness of the fixed support model, h = structure height, k_x = foundation transition stiffness and k_θ = foundation rotation stiffness. Transitional and rotational stiffness of the foundation

were calculated according to the geotechnical report in Table 3. For this purpose, the equivalent modulus of elasticity was estimated as 34.32 MPa by using the weight averaging of the elasticity modulus of various soil layers. The dimensions of foundation have been taken 9 m × 14 m. Finally, the ratio of the period of the SSI model to the fixed support model equals 3.27. It is observed that the period ratio derived by the ASCE 7–16 is in good consonant with the results of numerical analysis.
A comparison between the capacity curves of the structure was performed in both situations, considering the SSI and the fixed support models. Figure 16 shows the capacity curves from the pushover analysis. On each response curve, three different points A, B, and C are marked; structure yielding occurrence (A); appearance of maximum tensile stress at the heel of the masonry wall, ε_{tu} = 0.15%, which is accompanied through an obvious alter in the diagram slope (B), and the peak displacement value (C). As shown in Fig. 16, the SSI effects produce a reduction of base shear and initial stiffness, and increases the displacement capacity. The effects of SSI in the X-direction reduces 68.7% and 69.9% of the base shear at the yield and collapse states, respectively, as well as increases 3.66 and 5.17 times the displacement at the yield and collapse points. In addition, for direction Z, SSI reduces 71.7% and 63.8% of the base shear at the yield and collapse states, respectively, as well as increases 1.49 and 2.11 times the corresponding displacements. As expected, the soil compliance has a higher impact within the X-direction due to the greater stiffness provided by the piers' presence.

Table 7
Vibration periods of common modes.

Mode	Base condition	Period (s)	Period ratio
1	Fixed support	0.093	2.32
1	SSI	0.216	
5	Fixed support	0.054	3.26
3	SSI	0.176	

Figure 17 shows the progress of damage by increasing load in three stages corresponding to points A, B, and C on the pushover curves. According to Fig. 17, the damage onset is accompanied by tension cracks in the footwall joint. Then, in the X-direction, by creating cracks on the right and left sides of the short arch and dome, the dome and the short arch collapse and finally the whole structure are destroyed by the overturning of the pier walls. In the Z-direction, with the growth of cracks in the area of the bearing walls-long arch-short arc-dome and their connection to each other, as well as the appearing the cracks in the connection of the short arc to the wall, the entire roof of the Bazaar collapsed and the entire structure is destroyed by the overturning of the masonry walls. In the fixed support model, it is observed that the damage is more distributed in the entire structure because of the rigid base condition. The results of analyses indicate that plastic points and damage distribution are fundamentally modified by the SSI effects. As a consequence, the flexible foundation affects substantially the tension strain arrangement and afterwards the local failure mechanisms.

Figure 18 compares the capacity spectrum and the demand spectrum within the ADRS style. As shown, in design-basis earthquake demand, the fixed support model continues linearly in the X-direction whereas it hardly withstands against collapsing in the Z-direction. However, the SSI model collapses completely under the DBE demand. Moreover, the structure does not have the required capacity for MCE demand at all. Comparing the results of the fixed support model with the SSI case shows that the soil deformability leads to increment displacement, reduce base shear and factor of safety. Thus, the above-mentioned numerical simulations illustrate that the SSI effects are damaging to the structure seismic behavior, and the SSI omission overestimates the structure capacity and induces irrational responses.

For the given ground motion records, Fig. 19 shows the distribution of tensile damage in two models, fixed support and SSI cases. According to this Figure, the state of the structure in the fixed support model is better than the SSI model. Due to the Duzce and Tottori records, the structure maintains its stability and it is destroyed under the Manjil record. It is observed that the state of the structure in the SSI model is critical, so that the structure goes under complete collapse under all ground motion records. This time history results can be considered quietly match with the results of N2 method, which confirm each other. Examining the form of damage, it can be concluded that the destruction progress of the structure under all three records is as

follows: The collapse of the dome with a short arc and then the collapse of the long arc, and finally the overthrow of the upright walls. The validity of these results is increased by comparing them with the pushover results in Fig. 20. As shown in Fig. 20, the damage distribution has many similarities in time history analysis and pushover procedure. So that, damage in time history analysis is a collection of damage in both directions X and Z. Since the structure is subjected to earthquake record components in both directions, this result is rational. Generally, it can be expressed that the structure collapse is not only due to the growth of cracks in each area but also due to the joining of the cracks, which causes the failure of the whole structure. As mentioned before, this is due to the fact that the continuous and interconnected performance in the force transition system has a key part for the Bazaar structure stability.

The base shear using time history analysis for the selected seismic record set is shown in Fig. 21. According to this Figure, the foundation flexibility reduces the base shear compared to the corresponding fixed support model. The value of this decrease for the Duzce record in the directions X and Z is respectively, -4.4% and 44.8%; for the Manjil record in the directions X and Z is respectively, 48.8% and 65.2%; and for the Tottori record in the directions X and Z is respectively, 79.5% and 67.0%. The maximum base shear from the pushover analysis for each direction is also shown as a horizontal line in the diagrams. It is observed that the maximum base shear time history is less than the maximum base shear from the pushover analyses, except in SSI model where, depending on the ground motion record, the base shear time history may go more than the maximum base shear in the pushover analysis (Fig. 21a).

Figure 22 compares the displacement time histories due to the considered ground motion records. According to this Figure, in the fixed support model, the displacement time histories are less than the pushover procedure. For the SSI model, the displacement values have increased to such an extent that in some places it reached the displacements from the pushover analysis. In the case of a fixed support, the displacement of the X-axis is much less than the Z-axis; however, in the model considering SSI, this difference is not observed. It is noted that such pattern was also observed in the pushover capacity curves as discussed earlier. In addition, the displacement value in the SSI model has increased compared to the fixed support model. This increase for the Duzce ground motion record in the directions X and Z is respectively, 9.43 and 5.28 times. For the Manjil record in the directions X and Z is respectively, 8.19 and 6.57 times. For the Tottori record in the directions X and Z is respectively, 3.87 and 3.05 times.

7. Conclusions

The seismic behavior and failure mechanism of the historical structure of Kashan Grand Bazaar was assessed by considering the effects of SSI. Modal, nonlinear time history and pushover analyses were carried out using detailed 3D finite element models. The masonry and soil medium have been considered by the damage plasticity and the Mohr-Coulomb material models, respectively. The validity of the numerical method was evaluated by comparison with experimental results. The main conclusions are as follows:

- Soil compliance affects significantly the vibration periods and mode shapes, where the fundamental period of the SSI model was amplified up to 2.32 times compared to the fixed support case.
- For DBE demand, the fixed support model sustains stability in the X-direction whereas it hardly withstands against collapse in the Z-direction. The SSI model collapses completely under the DBE demand. Also, both structure models do not have the required capacity for MCE demand.
- The failure mechanism and damage distribution were essentially influenced by foundation flexibility. The collapse of the structure is not only due to the growth of cracks in each component, such as dome, short arcs, long arcs, and piers, but also due to the joining of the cracks in the force transition system.
- From pushover analysis, considering SSI caused a decrease of 70% in the ultimate base shear and an increase of up to 5.17 times in the displacement demands.
- From time history analyses, considering SSI reduced the base shear as much as 80% and increased the displacement up to 9.43 times. Thus, in time history analysis, less base shear and more displacement values were obtained rather than in pushover analysis.

- The SSI is detrimental to the structure behavior against earthquake loading, and its omission overestimates the structure capacity and induces irrational responses.

As described, the obtained results of this study are useful to evaluate the SSI effects on the seismic behavior of heritage structures. However, the employed numerical model still needs verification against additional experimental studies such as mechanical properties of masonry and field pushover tests in order to generalize the findings for retrofitting recommendations.

Declarations

Acknowledgements

The authors would like to appreciate the cooperation of the Municipality as well as the Cultural Heritage, Tourism and Handicrafts Organization of Kashan on the research illustrated in the article.

References

1. Feilden B (2007) Conservation of historic buildings. Routledge
2. Silva LC, Mendes N, Lourenço PB, Ingham J (2018) Seismic structural assessment of the Christchurch Catholic Basilica, New Zealand, vol 15. Structures, pp 115–130. doi:10.1016/j.istruc.2018.06.004
3. Machat C, Ziesemer J (2017) *Heritage at risk: ICOMOS World Report 20142015 on Monuments and Sites in Danger* (C. Machat and J. Ziesemer Eds. 1., Erstausgabe ed.). Berlin: Bäßler, H
4. Peña F, Lourenço PB, Mendes N, Oliveira DV (2010) Numerical models for the seismic assessment of an old masonry tower. Eng Struct 32(5):1466–1478. doi:10.1016/j.engstruct.2010.01.027
5. Valente M, Milani G (2016) Seismic assessment of historical masonry towers by means of simplified approaches and standard FEM. Constr Build Mater 108:74–104
6. Roque J, Oliveira DV, Ferreira TM, Lourenço PB (2019) Nonlinear dynamic analysis for safety assessment of heritage buildings: Church of Santa Maria de Belem. J Struct Eng 145(12):04019153
7. Aghabeigi P, Mahmoudi R, Ahani E, Hosseinian Ahangarnazhad B (2021) Seismic assessment and retrofitting of the masonry building of mozaffarieh timche in tabriz historic bazaar. Int J Architectural Herit 15(12):1816–1841
8. Aghabeigi P, Farahmand-Tabar S (2021) Seismic vulnerability assessment and retrofitting of historic masonry building of Malek Timche in Tabriz Grand Bazaar. Eng Struct 240:112418
9. Page AW (1978) Finite element model for masonry. J Struct Div 104(8):1267–1285
10. Lourenço PB, Rots JG, Feenstra PH (1995) A tensile “Rankine” type orthotropic model for masonry. Comput methods Struct Mason 3:167–176
11. Lourenço PB (1997) *Computational strategies for masonry structures*
12. Marques R, Lourenço PB (2014) Unreinforced and confined masonry buildings in seismic regions: Validation of macro-element models and cost analysis. Eng Struct 64:52–67
13. Zizi M, Chisari C, Rouhi J, De Matteis G (2022) *Comparative analysis on macroscale material models for the prediction of masonry in-plane behavior*. Bulletin of Earthquake Engineering, 20(2), 963–996
14. Kramer SL (1996) Geotechnical earthquake engineering. Prentice Hall, Upper Saddle River, NJ
15. Tahghighi H, Rabiee M (2017) Influence of foundation flexibility on the seismic response of low-to-mid-rise moment resisting frame buildings. Int J Sci Technol SCIENTIA IRANICA 24(3):979–992
16. Tahghighi H, Mohamadi A (2020) Numerical evaluation of soil-structure interaction effects on the seismic performance and vulnerability of reinforced concrete buildings. Int J Geomech 20(6):04020072. https://doi.org/10.1061/(ASCE)GM.1943-5622.0001651
17. Piro A, de Silva F, Parisi F, di Santolo S, Silvestri F (2020) *Effects of soil-foundation-structure interaction on fundamental frequency and radiation damping ratio of historical masonry building sub-structures*. Bulletin of Earthquake Engineering,

18(4), 1187–1212
18. Tahghighi H, Konagai K (2007) Numerical analysis of nonlinear soil–pile group interaction under lateral loads. Soil Dyn Earthq Eng 27(5):463–474
19. Far H (2019) Advanced computation methods for soil-structure interaction analysis of structures resting on soft soils. Int J Geotech Eng 13(4):352–359
20. Tabatabaiefar HR, Fatahi B, Ghabraie K, Zhou W (2015) Evaluation of Numerical Procedures to Determine Seismic Response of Structures under Influence of Soil-Structure Interaction. Struct Eng Mech 56(1):27–47
21. Sharari N, Fatahi B, Hokmabadi AS, Xu R (2022) Impacts of Pile Foundation Arrangement on Seismic Response of LNG Tanks Considering Soil–Foundation–Structure Interaction. J Perform Constr Facil 36(1):04021110
22. Housner GW (1957) Interaction of building and ground during an earthquake. Bull Seismological Soc Am 47:179–186
23. Maria CR, Sebastiano F, Renato L, Donato S (2015) Dynamic behavior of shallow founded historic towers: validation of simplified approaches for seismic analyses. Int J Geotech Eng 9(1):13–29. doi:10.1179/1939787914Y.0000000066
24. de Silva F, Ceroni F, Sica S, Pecce M, Silvestri F (2015) Effects of soil-foundation-structure interaction on the seismic behavior of monumental towers: The case study of the Carmine Bell Tower in Naples. Rivista Italiana di Geotecnica 49(3):7–27
25. Güllü H, Jaf HS (2016) Full 3D nonlinear time history analysis of dynamic soil–structure interaction for a historical masonry arch bridge. Environ Earth Sci 75(21):1421. doi:10.1007/s12665-016-6230-0
26. Fathi A, Sadeghi A, Emami Azadi MR, Hoveidaie N (2020) Assessing seismic behavior of a masonry historic building considering soil-foundation-structure interaction (Case Study of Arge-Tabriz). Int J Architectural Herit 14(6):795–810
27. Fathi A, Sadeghi A, Emami Azadi MR, Hoveidae N (2020) Assessing the soil-structure interaction effects by direct method on the out-of-plane behavior of masonry structures (case study: Arge-Tabriz). Bull Earthq Eng 18(14):6429–6443
28. Hökelekli E, Al-Helwani A (2020) Effect of soil properties on the seismic damage assessment of historical masonry minaret–soil interaction systems. Struct Des Tall Special Build 29(2):e1694. doi:10.1002/tal.1694
29. de Silva F (2020) Influence of soil-structure interaction on the site-specific seismic demand to masonry towers. Soil Dyn Earthq Eng 131:106023. doi:https://doi.org/10.1016/j.soildyn.2019.106023
30. Systemes D (2019) *SolidWorks* (Version 2019): Dassault Systemes
31. Systemes D (2014) *Abaqus* (Version 6.14). Dassault Systemes
32. Karimi MS, Moradi E, Mehri T (2015) *Bazaar, as a symbol of culture and the architecture of commercial spaces in Iranian-Islamic civilization*.Fen Bilimleri Dergisi (CFD), 36(6)
33. Google (Cartographer) (2019a) *Location of Kashan Bazaar*. Retrieved from https://shorturl.at/bkBKR
34. Google (Cartographer) (2019b) *Location of Iran*. Retrieved from https://shorturl.at/qtvLW
35. Ambraseys NN, Melville CP (1982) A history of Persian earthquake. Cambridge University Press
36. Golabchi M, Javani Dizaji A (2018) Iranian architecture technology. University of Tehran Press, Tehran, Iran. (In Persian)
37. NTC (2008) Technical standards for construction. Ministry of Infrastructure and Transport, Italy
38. Degli Abbati S, D'Altri AM, Ottonelli D, Castellazzi G, Cattari S, de Miranda S, Lagomarsino S (2019) Seismic assessment of interacting structural units in complex historic masonry constructions by nonlinear static analyses. Comput Struct 213:51–71. doi:10.1016/j.compstruc.2018.12.001
39. Valente M, Milani G (2016) Nonlinear dynamic and static analyses on eight historical masonry towers in the North-East of Italy. Eng Struct 114:241–270. doi:10.1016/j.engstruct.2016.02.004
40. Lee J, Fenves GL (1998) Plastic-damage model for cyclic loading of concrete structures. J Eng Mech 124(8):892–900. doi:doi:
10.1061/
(ASCE)0733-9399(1998)124:8(892)
41. Lubliner J, Oliver J, Oller S, Oñate E (1989) A plastic-damage model for concrete. Int J Solids Struct 25(3):299–326. doi:10.1016/0020-7683(89)90050-4

42. Hillerborg A, Modéer M, Petersson PE (1976) Analysis of crack formation and crack growth in concrete by means of fracture mechanics and finite elements. Cem Concr Res 6(6):773–781. doi:https://doi.org/10.1016/0008-8846(76)90007-7
43. Karimi AH, Karimi MS, Kheyroddin A, Shahkarami AA (2016) Experimental and numerical study on seismic behavior of an infilled masonry wall compared to an arched masonry wall. Structures 8:144–153. doi:10.1016/j.istruc.2016.09.012
44. Karimi AH, Karimi MS, Kheyroddin A, Amirshahkarami A (2017) Nonlinear modeling of unreinforced masonry wall under in-plane load and investigation of the effect of various parameters. J Struct Constr Eng 3(4):21–34
45. Municipality of Kashan (2010) Geotechnical investigations report of Bab al-Huaij multi-story parking building site in Kashan Bazaar region. Soil Mechanics Laboratory, Islamic Azad University, Kashan, Iran. (In Persian)
46. Coulomb C (1776) Essai sur une application des rèles des maximis et minimis a quelques problems de statique, vol 7. Memoires Acad. Royale des Sciences
47. Jin YF, Zhu BQ, Yin ZY, Zhang DM (2019) Three-dimensional numerical analysis of the interaction of two crossing tunnels in soft clay. Undergr Space 4(4):310–327. doi:10.1016/j.undsp.2019.04.002
48. Yang X, Yang G, Yu T (2012) Comparison of strength reduction method for slope stability analysis based on Abaqus FEM and FLAC3d FDM. Applied Mechanics and Materials
49. de Silva F, Ceroni F, Sica S, Silvestri F (2018) Nonlinear analysis of the Carmine bell tower under seismic actions accounting for soil–foundation–structure interaction. Bull Earthq Eng 16(7):2775–2808. doi:10.1007/s10518-017-0298-0
50. Ghadimi Chermahini A, Tahghighi H (2019) Numerical finite element analysis of underground tunnel crossing an active reverse fault: a case study on the Sabzkouh segmental tunnel. Geomech Geoeng 14(3):155–166. doi:10.1080/17486025.2019.1573323
51. Schneider CA, Rasband WS, Eliceiri KW (2012) NIH Image to ImageJ: 25 years of image analysis. Nat Methods 9(7):671. doi:10.3410/f.717951500.793456800
52. Salih Y, Malik AS (2012) *Depth and geometry from a single 2d image using triangulation*. 2012 IEEE International Conference on Multimedia and Expo Workshops, Melbourne, VIC, Australia
53. Ghosh S, Wilson EL (1969) Dynamic stress analysis of axi-symmetric structures under arbitrary loading. University of California, California, Berkeley
54. Lagomarsino S, Cattari S (2015) PERPETUATE guidelines for seismic performance-based assessment of cultural heritage masonry structures. Bull Earthq Eng 13(1):13–47. doi:10.1007/s10518-014-9674-1
55. Castellazzi G, D'Altri AM, de Miranda S, Ubertini F (2017) *An innovative numerical modeling strategy for the structural analysis of historical monumental buildings*. Engineering Structures, 132, 229–248
56. Acito M, Bocciarelli M, Chesi C, Milani G (2014) Collapse of the clock tower in Finale Emilia after the May 2012 Emilia Romagna earthquake sequence: Numerical insight. Eng Struct 72:70–91. doi:10.1016/j.engstruct.2014.04.026
57. Acito M, Chesi C, Milani G, Torri S (2016) Collapse analysis of the Clock and Fortified towers of Finale Emilia, Italy, after the 2012 Emilia Romagna seismic sequence: Lesson learned and reconstruction hypotheses. Constr Build Mater 115:193–213. doi:10.1016/j.conbuildmat.2016.03.220
58. Fajfar P (1999) Capacity spectrum method based on inelastic demand spectra. Earthq Eng Struct Dynamics 28(9):979–993
59. Standard 2800 (2015) *Iranian code of practice for seismic resistance design of buildings*. 4th Revision, Building and Housing Research Center, Tehran, Iran
60. PEER (2020) *Strong motion database*. Pacific Earthquake Engineering Research Center. University of California, Berkeley, CA, USA. http://peer.berkeley.edu
61. Tehran Padir Consultant Engineering (2012) A comprehensive report for seismic microzonation and vulnerability of Kashan, Iran. Prepared by Isfahan Housing and Urban Development Organization, Isfahan, Iran. (In Persian)
62. Hashash YMA, Musgrove MI, Harmon JA, Ilhan O, Xing G, Groholski D, Phillips CA, Park D (2020) DEEPSOIL V7.0, User Manual. Board of Trustees of University of Illinois at Urbana-Champaign, IL., USA, Urbana, IL
63. ASCE 7 (2016) *Minimum design loads for buildings and other structures*. ASCE/SEI 7–16. American Society of Civil Engineers/Structural Engineering Institute, Reston, VA, USA

Figures

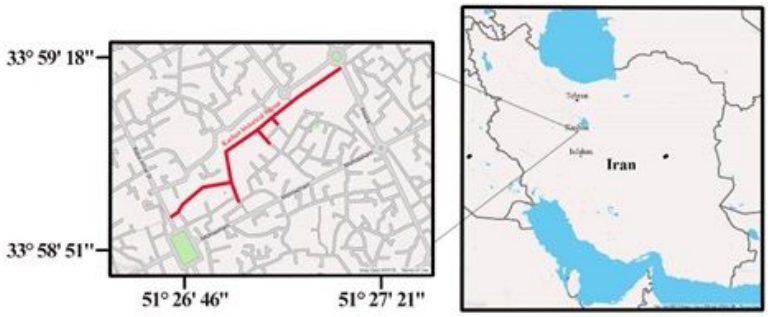

Figure 1

The case study geographical location [33, 34]

Figure 2

A general view of the Bazaar interior.

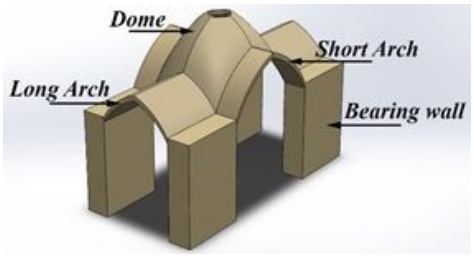

Figure 3

Typical components of the Bazaar structure.

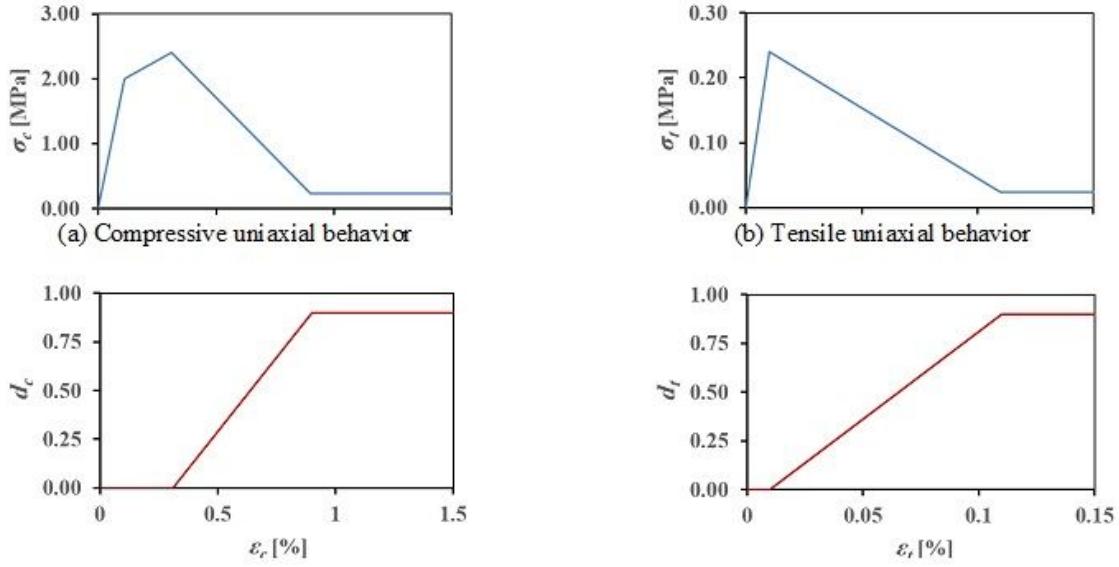

Figure 4

Constitutive laws for masonry.

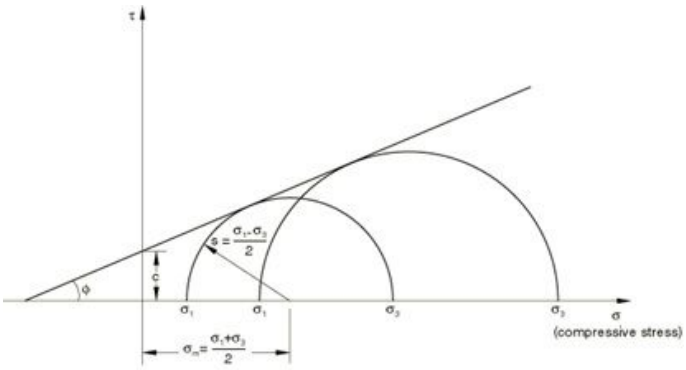

Figure 5

Mohr-Coulomb shear failure criterion [46]

Figure 6

3D view of the finite element models: (a) Without SSI, and (b) With SSI.

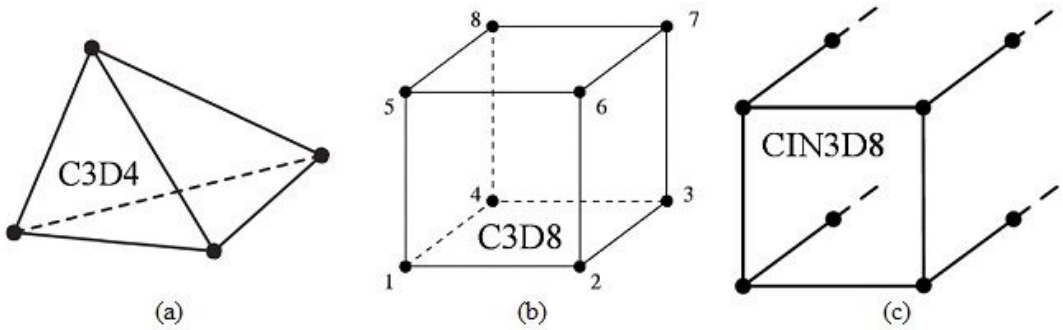

Figure 7

Finite and infinite elements used in this study: (a) C3D4, (b) C3D8, and (c) CIN3D8

Figure 8

Masonry wall numerical model.

Figure 9

Hysteretic curves of numerical study and experiment results.

Figure 10

Envelope curves of experiment and numerical analyses results.

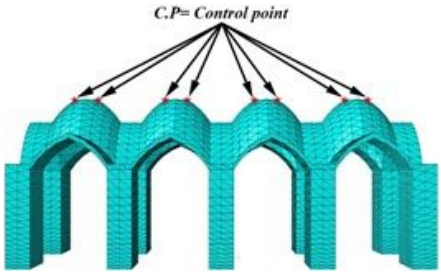

Figure 11

Displacement control points in the pushover analysis.

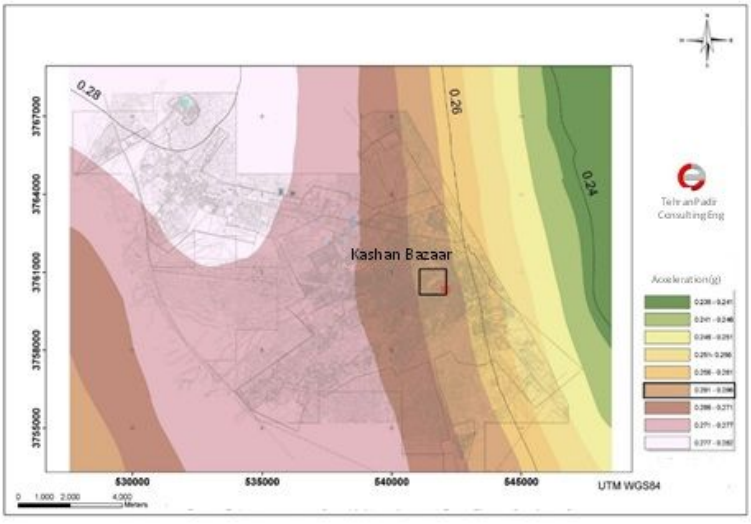

Figure 12

Seismic hazard map of Kashan city for the 10% exceedance probability in 50 years (DBE), expressed in terms of the PGA parameter on seismic bedrock (after [61]).

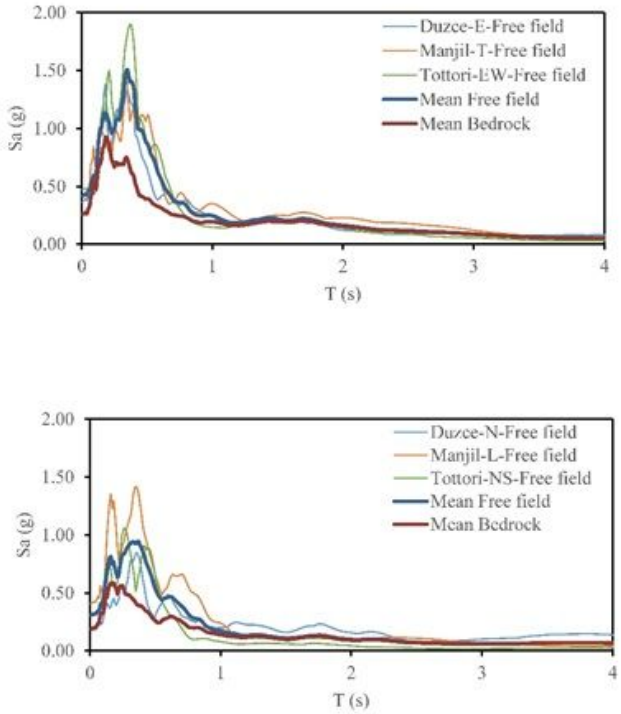

Figure 13

Acceleration response spectra of scaled records (bedrock and free field): (a) X-direction, and (b) Y-direction.

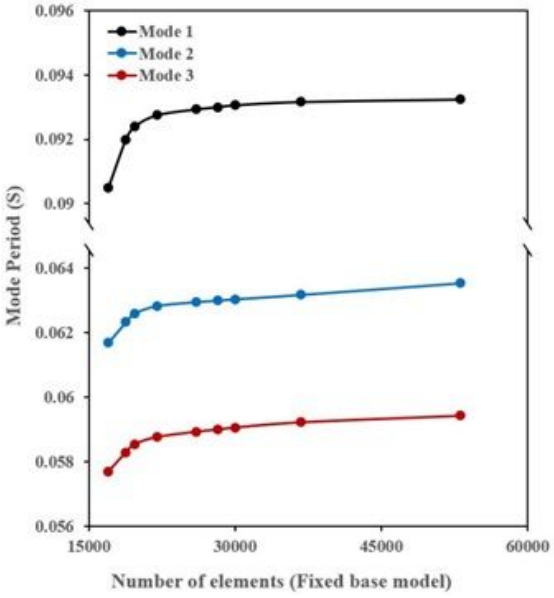

Figure 14

Vibration period of the first three modes in terms of finite element numbers (fixed support model).

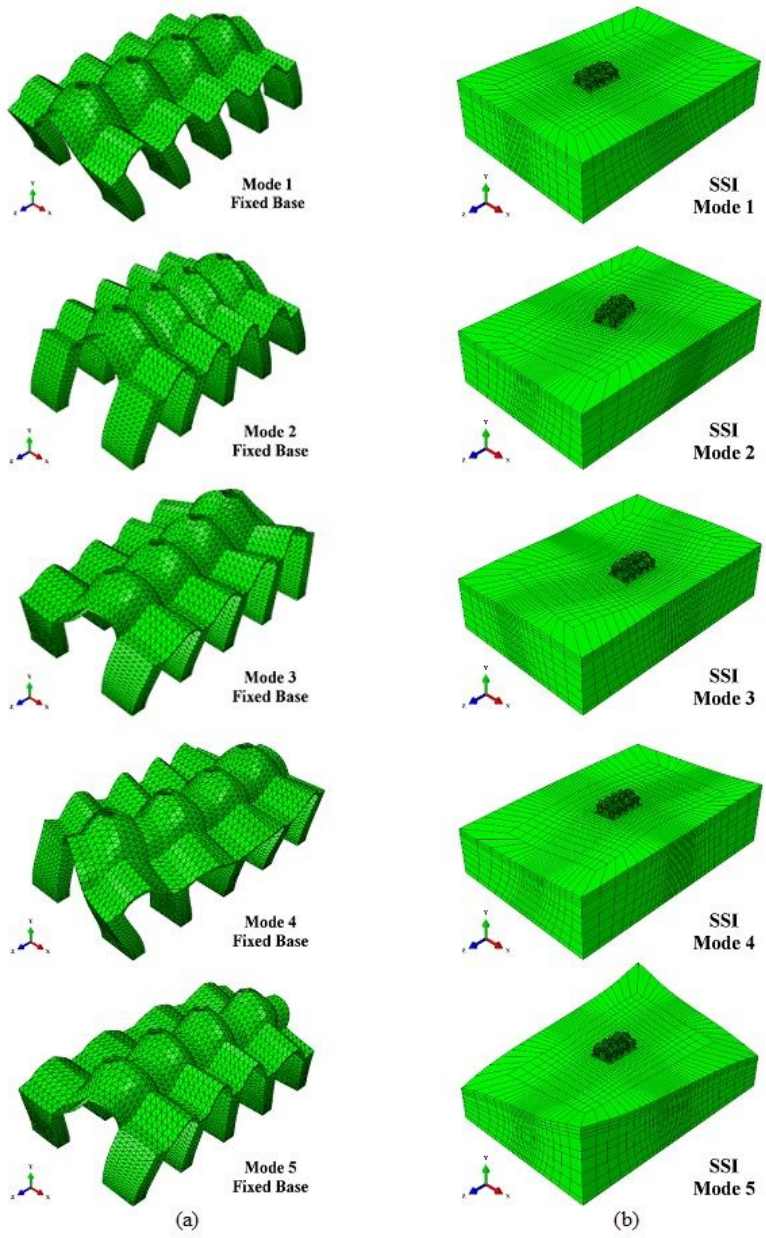

Figure 15

The first five shape modes: (a) Fixed support model, and (b) SSI model.

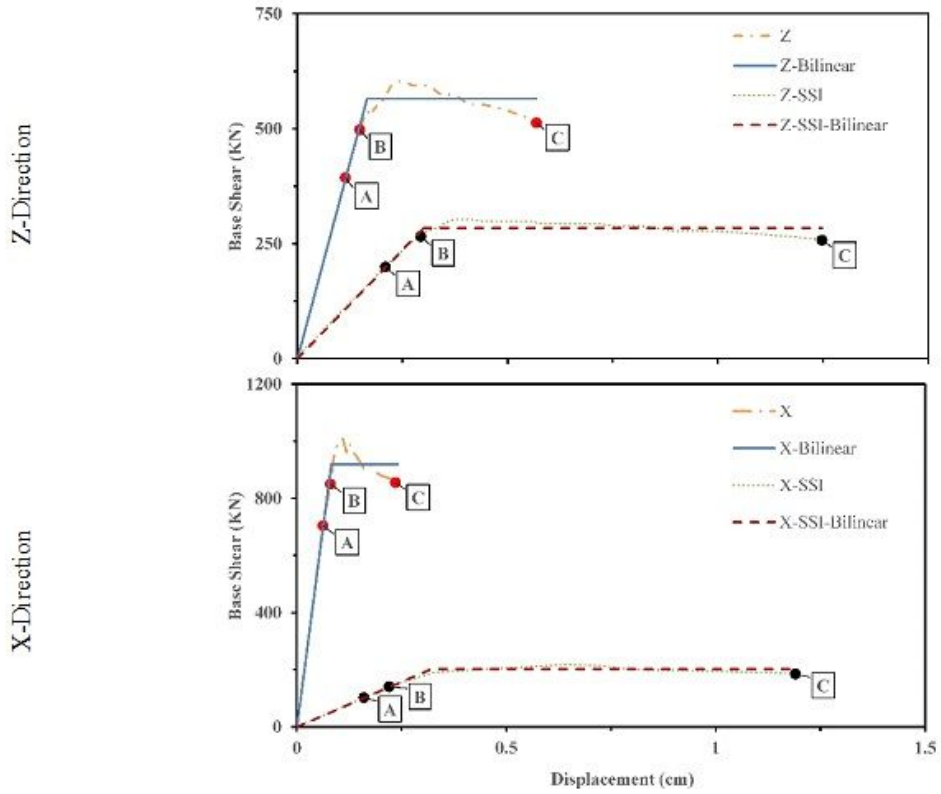

Figure 16

Capacity curves in the axes X and Z (with and without SSI).

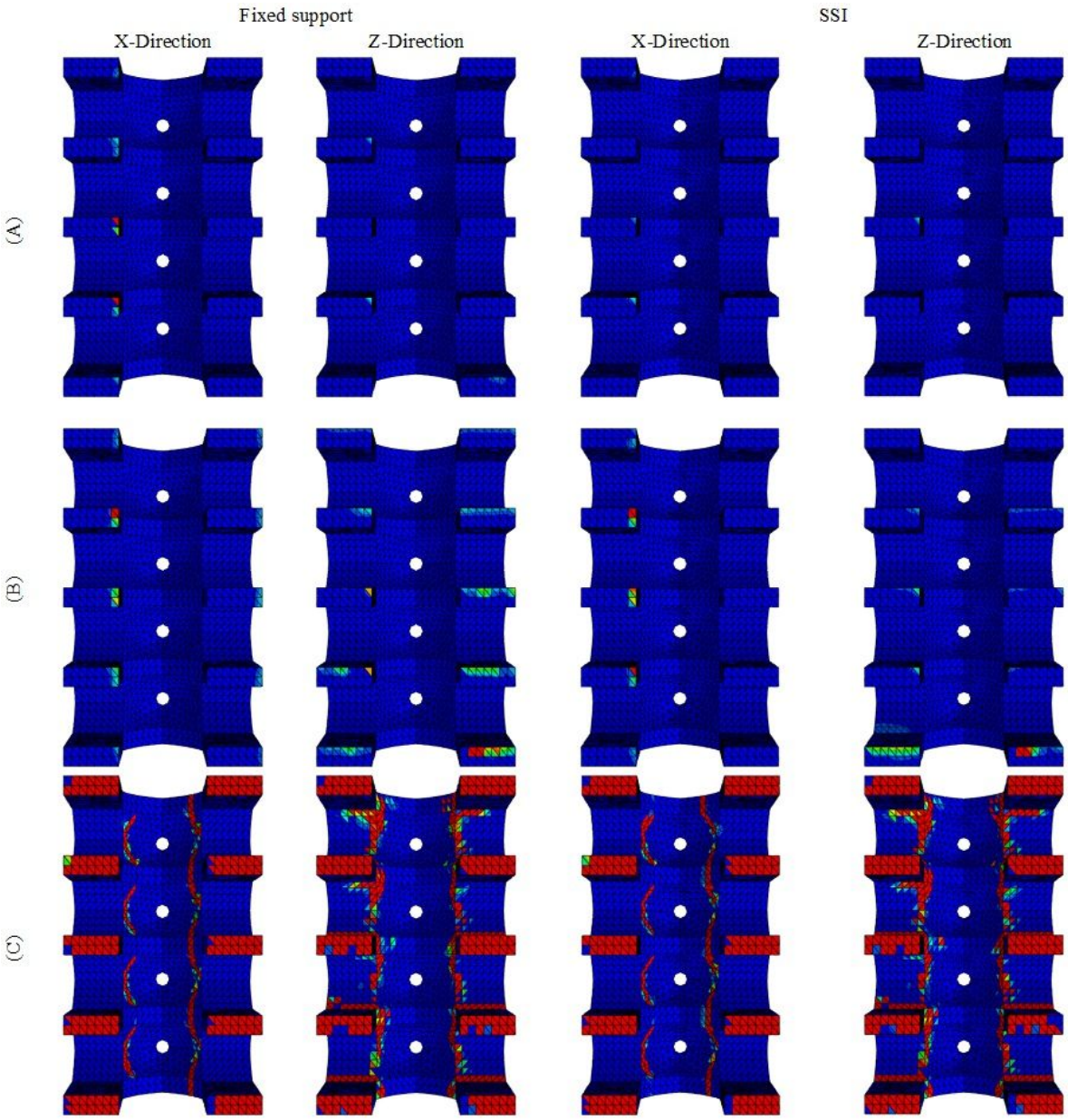

Figure 17

Damage progress of the structure model in directions X and Z (with and without SSI).

Figure 18

Demand versus capacity spectra in directions X and Z for models with and without SSI under DBE and MCE hazard levels.

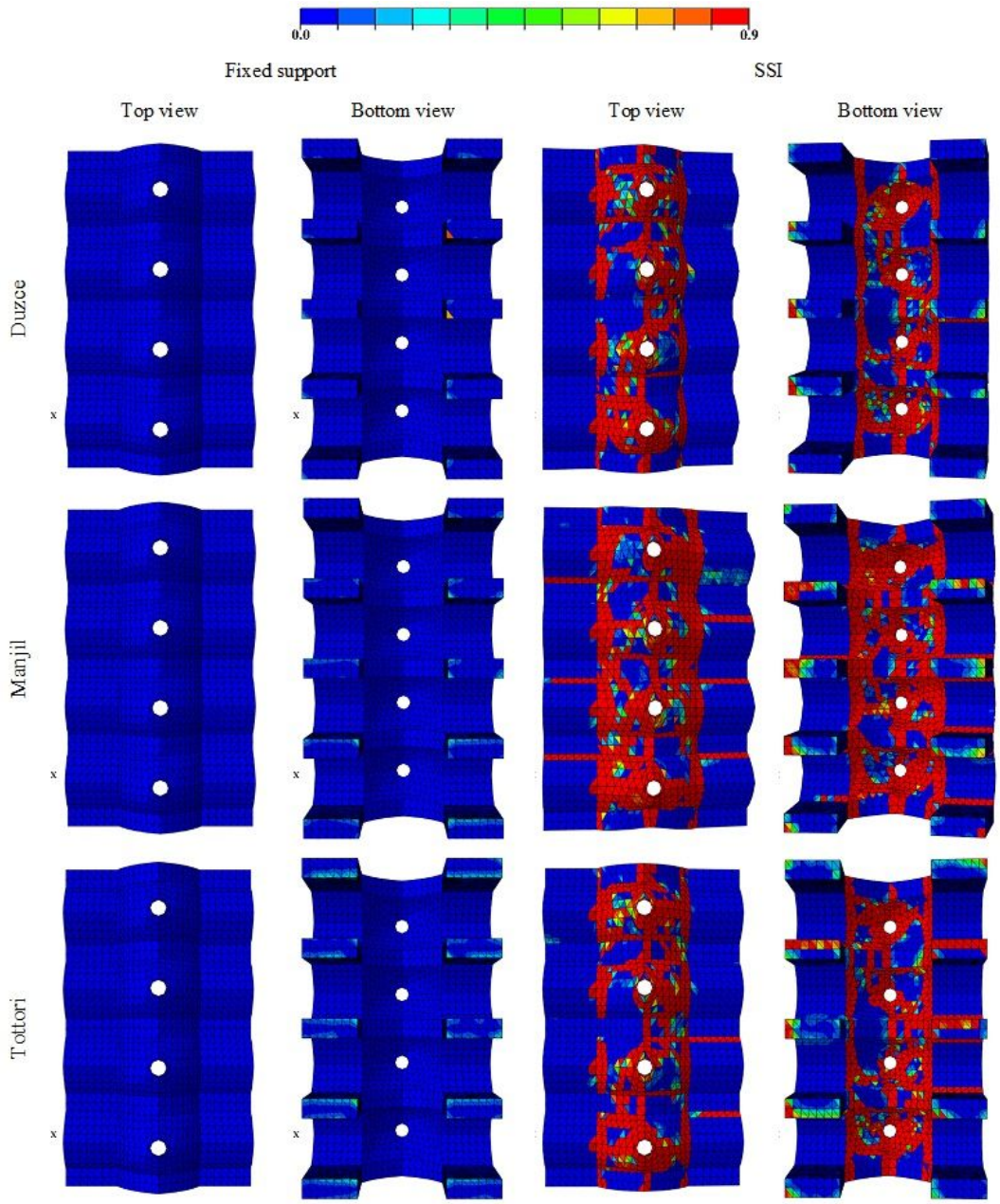

Figure 19

Tensile damage distribution due to earthquake records for fixed support and SSI models (Top view and Bottom view)

Figure 20

Comparison between the damage distributions for fixed support and SSI models: (a) Pushover procedure, and (b) nonlinear time history analysis.

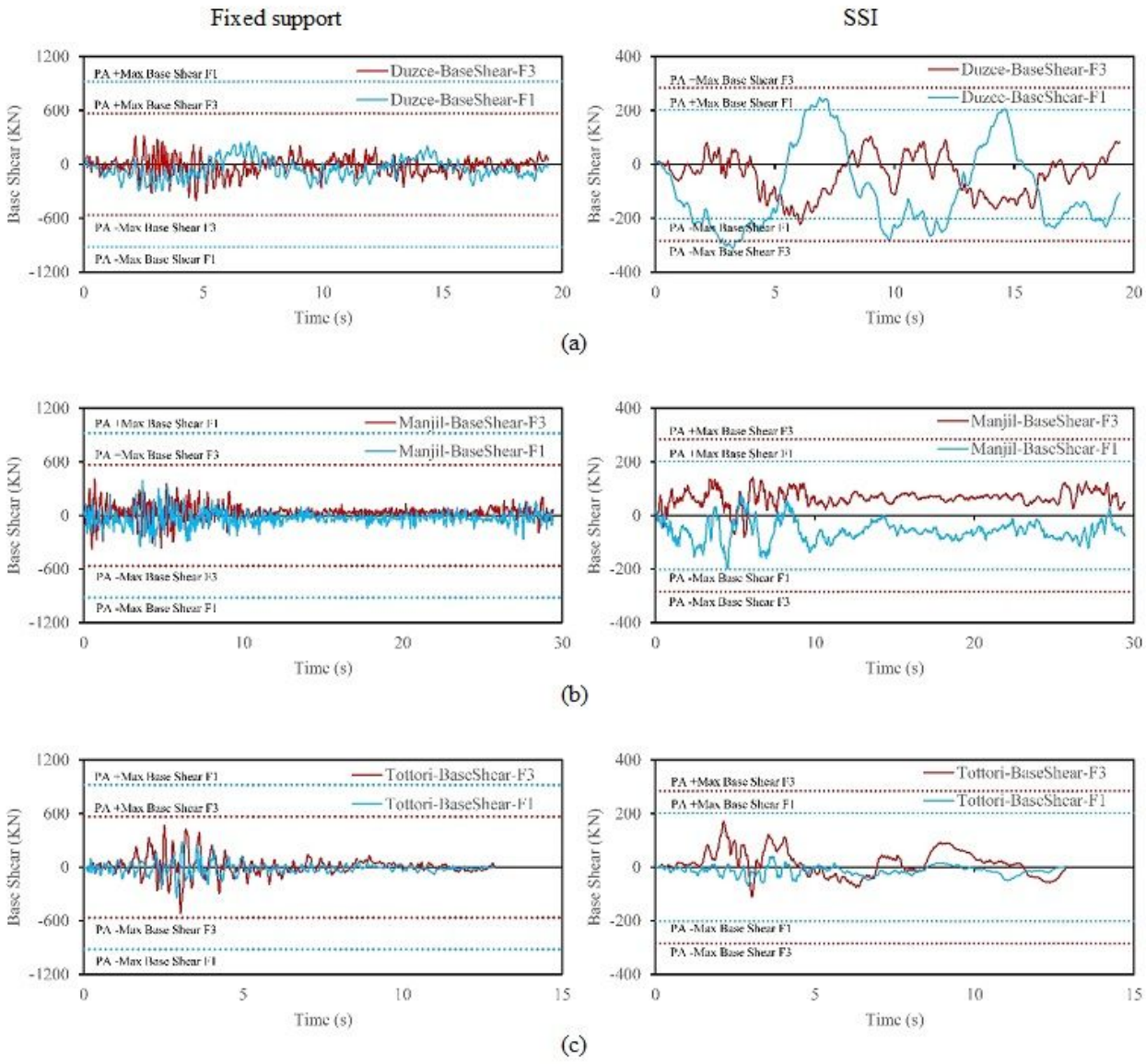

Figure 21

Comparison between base shear time histories in the axes X and Z for models with and without SSI: (a) Duzce record, (b) Manjil record, and (c) Tottori record.

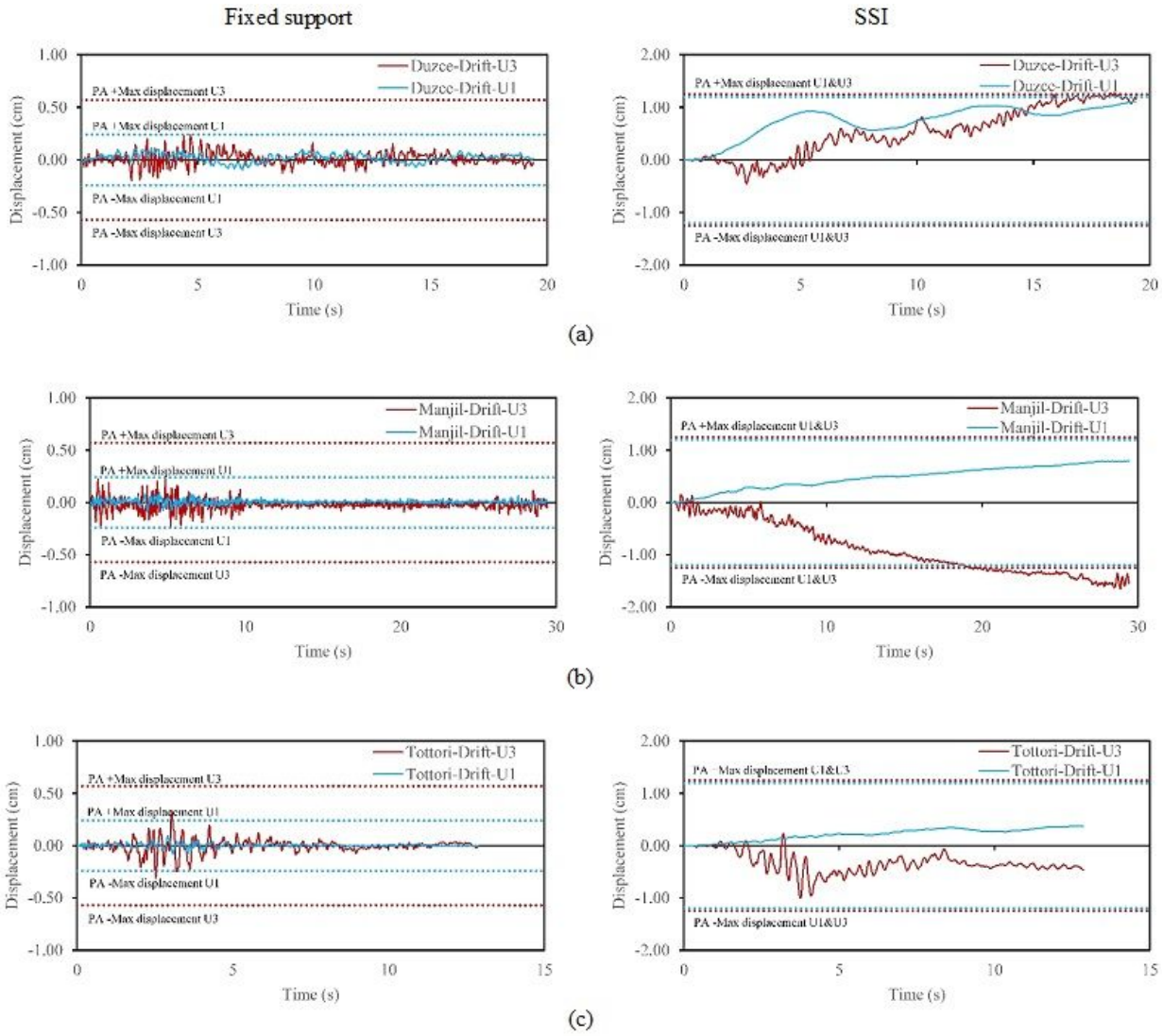

Figure 22: Comparison between displacement time histories in the axes X and Z for models with and without SSI: (a) Duzce record, (b) Manjil record, and (c) Tottori record.

Figure 22

Comparison between displacement time histories in the axes X and Z for models with and without SSI: (a) Duzce record, (b) Manjil record, and (c) Tottori record